Journal of Computational Physics **172,** 640–657 (2001)
doi:10.1006/jcph.2001.6846, available online at http://www.idealibrary.com on IDEAL®

Numerical Simulation of the Slider Air Bearing Problem of Hard Disk Drives by Two Multidimensional Upwind Residual Distribution Schemes over Unstructured Triangular Meshes

Lin Wu and D. B. Bogy

Computer Mechanics Laboratory, Department of Mechanical Engineering, University of California at Berkeley, Berkeley, California 94720
E-mail: linwu@newton.berkeley.edu.dbogy@cml.me.berkeley.edu

Received June 26, 2000; revised May 29, 2001

In this paper we present two multigrid numerical schemes over unstructured triangular meshes that solve the slider air bearing problem of hard disk drives. For each fixed slider attitude, the air bearing pressure is obtained by solving the generalized Reynolds equation. The convection part of the equation is modeled in one scheme by the PSI multidimensional upwind residual distribution approach and in the other scheme by the SUPG finite element approach cast in residual distribution form. In both schemes, a linear Galerkin method is used to discretize the diffusion terms. In addition, a non-nested multigrid iteration technique is used to speed up the convergence rate. Finally, the balanced steady state flying attitude of the slider subject to pre-applied suspension force and torques is obtained by a Quasi–Newton iteration method (Broyden's method), and the results of the numerical solutions are compared to each other and to experimental data. © 2001 Academic Press

Key Words: air bearing; finite elements; hard disk drive; mesh generation and refinement; rarefied gas flows; residual distribution scheme; unstructured meshes.

1. INTRODUCTION

In today's hard disk drive (Fig. 1), the read–write element is attached to the trailing edge of an air bearing slider (Figs. 2–4). This slider glides over the rotating disk with a separation (flying height) determined by the balance between the air bearing force and moments generated by the extremely thin squeezed air layer under the slider and the opposing force and moments exerted by a pre-load of the suspension, which links the slider and the actuator (Fig. 2). The slider has three degrees of freedom. It can move up and down and rotate around the point where the suspension is attached (Fig. 2) in the pitch and roll directions; the skew

0021-9991/01 $35.00

FIG. 1. The IBM Travelstar 25GB hard disk drive.

angle at each radial position is generally fixed. The distance between the read–write element and the disk surface where magnetic information is stored has significant influence on the read back signal. Fluctuation of the distance will cause noise in the read back signal. The suspension force and moments can be taken as constant values, but the air bearing force and moments have to be calculated from the generalized Reynolds equation obtained from the Boltzmann equation. To increase the storage density and reduce the signal noise, it is desirable to achieve a low and uniform steady state flying height across the disk. The design goal of the next generation hard disk drive is to reach an areal density of 100 Gbit/in^2, which requires a flying height between 5 and 10 nm. In the hard disk drive industry, the above flying attitude goal is obtained by carefully designing the air bearing surface of the slider, which generally has a very complicated shape. Figures 3 and 4 show one typical design. To reduce the design cost, accurate and efficient steady state air bearing design software is required.

In the slider's manufacturing process, the etching technique leaves a steep narrow wall profile region (a few microns wide and a few microns in recess depth from the air bearing surface for sliders with millimeter length scale) along the rail boundaries (Fig. 4). The

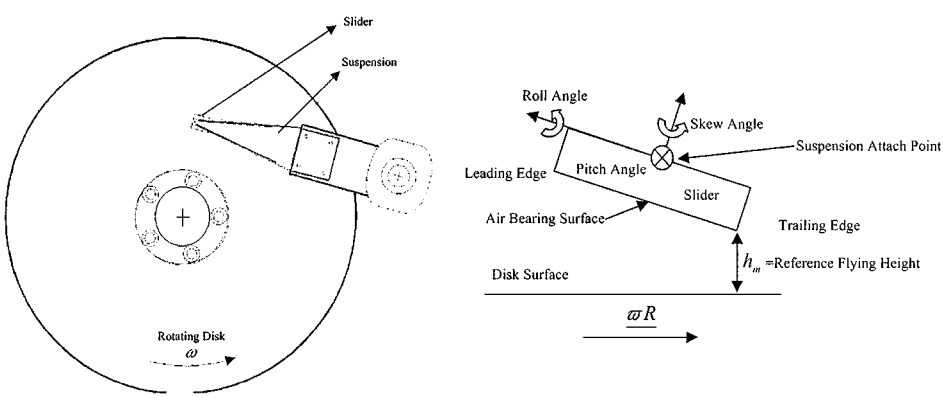

FIG. 2. A sketch of the hard disk drive assembly.

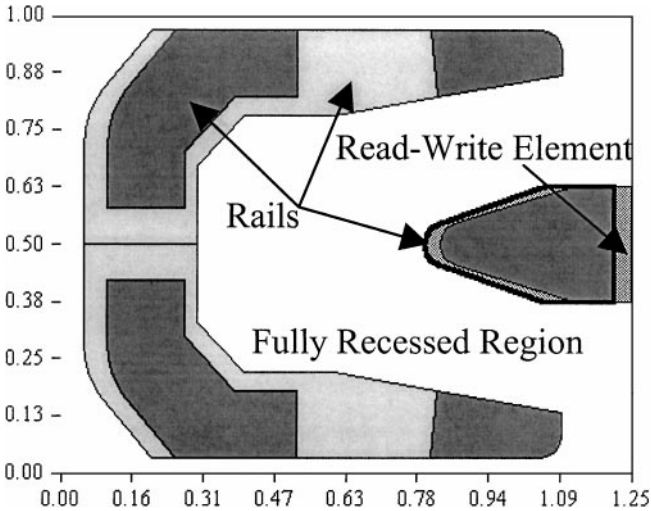

FIG. 3. The next generation NSIC (National Storage Industry Consortium) slider air bearing surface design with the left-hand side as the leading edge and the slider flying upside down with the suspension attached on its back. All scales have been normlized by the width (1 mm). Different color depth of the air bearing surface rails represents different recess depth from the top (air bearing surface).

dimensions and shape of the wall profiles have a profound influence on the flying attitude. As a result, it is important to accurately capture these regions of rapidly changing elevations in the numerical model. In addition, the air bearing pressure field is characterized by irregularly distributed regions with very high pressure gradient. To get accurate results, it is necessary to have fine enough grids to cover the above regions. Under these situations, unstructured grids prove to be an economical and convenient way of decomposing the computational domain.

In this paper we present two numerical schemes to solve the generalized Reynolds equation based on the unstructured triangular meshes generated by the Delaunay techniques

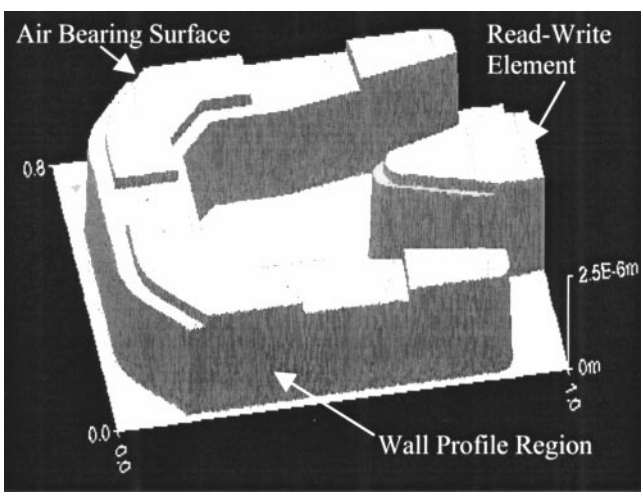

FIG. 4. The 3-D geometry of the NSIC slider. The horizontal scales have been normalized by the width (1 mm).

presented in our previous papers [1, 2]. The convection part of the generalized Reynolds equation is discretized by two different schemes—the positive streamwise invariant (PSI) residual distribution approach in [3, 4] and the streamline upwind Petrov-Galerkin (SUPG) finite element scheme [5] cast as a residual distribution formula [6]—while a standard linear Galerkin type method [7] is used to model the diffusion part of the equation. A non-nested multigrid technique based on the full storage approximation multi-grid strategy of Brandt [8] is implemented to improve the convergence rate of the Gauss–Seidel smoother used to solve the nonlinear discretized equation. Mavriplis and Jameson's restriction and interpolation functions [9] that suit non-nested triangular meshes are used to transfer the variables and residues between the meshes.

Finally, the balanced steady state flying height of the slider is found by a Quasi–Newton iteration method (Broyden's method) described in Dennis and Schnabel [10].

2. GOVERNING EQUATIONS AND BOUNDARY CONDITIONS

In air bearing simulation the generalized Reynolds equation is solved to get the pressure field. Because of the extremely narrow spacing between the slider and the disk (on the order of 10 nm, which is only a fraction of the mean free path of the gas molecules, about 65 nm under normal operating conditions), the gas in the spacing is extremely rarefied and the gas molecules at a solid surface no longer experience the same velocity as the surface, i.e., there is slipping. The usual continuum and nonslip condition assumptions no longer adequately describe the actual physics. Until now, the modified versions of the Reynolds equation that take the rarefaction and slipping effect into account give the most agreeable results with those of experiments and direct Monte Carlo simulation [11–15]. The different versions of the Reynolds equation can be written in a unified dimensionless form as

$$\sigma \frac{\partial}{\partial T}(PH) = \frac{\partial}{\partial X}\left(QPH^3 \frac{\partial P}{\partial X} - \Lambda_x PH\right) + \frac{\partial}{\partial Y}\left(QPH^3 \frac{\partial P}{\partial Y} - \Lambda_y PH\right), \tag{1}$$

where P, H, and T are the dimensionless pressure, distance between air bearing surface and disk surface and time, normalized by p_a, h_m and $1/\varpi$, respectively; p_a is the ambient pressure, h_m is the flying height of a reference point on the slider (usually taken to be the point at the trailing edge center of the slider assumed to have zero recess), ω is the constant angular velocity of the disk. The expression $\sigma = 12\mu\omega L^2/P_a h_m^2$ is the squeeze number, which represents the relative importance between the unsteady effect and the diffusion effect. The expressions $\Lambda_x = 6\mu UL/p_a h_m^2$ and $\Lambda_y = 6\mu VL/p_a h_m^2$ are the bearing numbers in the x- and y-directions, respectively, which represent the relative importance between the convection effect and the diffusion effect. The term μ is the dynamic viscosity of the gas, U and V are the disk velocity components in the x- and y-direction, and L is the length scale of the slider (taken here to be the width of the slider). The term Q is the flow factor, which marks the difference between different rarefaction and slip models of the equation. Different Q for different models can be found in Burgdorfer [11], Hsia and Domoto [12], and Fukui and Kaneko [13]. In our simulation, the Fukui–Kaneko model is used, which is the best model available when the air bearing clearance is below 100 NM [15]. In the implementation of the model, the database in [13] is used to find the flow factor. Along the outside boundary of the slider, the pressure is simply taken as the ambient pressure.

3. MESH GENERATION

Because of its geometric flexibility in constructing quality meshes around complex configurations and the relative convenience of incorporating an adaptive methodology, and also its efficiency and its ability to generate optimal connections to existing nodal points, a Delaunay method as described in [16] is used as a building block in our approach for the incremental mesh refinement and adaptation. Using different refinement techniques, we generate three sets of unstructured triangular meshes. For the coarsest meshes, it's important that the boundaries of the rails be represented in the triangulation, because the boundaries are the places with dramatic recess depth change. The conforming Delaunay refinement technique in Ruppert [17] is used to generate the coarsest conformed background meshes. The longest-side bisection Delaunay refinement technique in Rivara and Inostroza [18] is adopted to cluster fine meshes in the recess wall regions with rapid geometric change based on geometric considerations (the maximum recess depth difference in each triangle must be smaller than a prescribed value in order to model the rapid elevation change accurately), which forms the second finer meshes. For the final mesh adaptation, the maximum undivided pressure difference in a triangle is used to decide whether the triangle needs further refinement. The same longest-side bisection Delaunay refinement technique is used to refine the meshes. Details can be found in our previous papers [1, 2].

4. THE DISCRETIZATION OF THE CONVECTION EQUATION

Ignoring the diffusion terms in Eq. (1) for the moment and dividing the remaining terms by σ, we get the convection equation

$$\frac{\partial}{\partial T}(PH) + \frac{d}{dx}\left(\frac{\Lambda_x}{\sigma}PH\right) + \frac{d}{dy}\left(\frac{\Lambda_y}{\sigma}PH\right) = 0. \tag{2}$$

In the residual distribution schemes in [3, 4], the residual in triangle T is defined as

$$\begin{aligned}\phi^T &= -\iint_T \frac{\partial(PH)}{\partial T}\,dA = \iint_T \left(\frac{\Lambda_x}{\sigma}, \frac{\Lambda_y}{\sigma}\right)\cdot\nabla(PH)\,dA \\ &= A_T\bar{\lambda}_T\cdot\nabla(PH) = \sum_{j=1}^{3} k_j^T (PH)_j,\end{aligned} \tag{3}$$

where A_T is the area of the triangle and $\bar{\lambda}_T = (\overline{\Lambda_x, \Lambda_y})/\sigma$ is the averaged wave speed in each triangle. The conservation constraint gives

$$\bar{\lambda}_T = \frac{1}{A_T\sigma}\iint_T \left(\Lambda_x, \Lambda_y\right) dA = \frac{1}{3\sigma}[(\Lambda_x, \Lambda_y)_1 + (\Lambda_x, \Lambda_y)_2 + (\Lambda_x, \Lambda_y)_3]. \tag{4}$$

In the above formulation, the bearing number is assumed to vary linearly in each triangle. The inflow parameter k_j^T is defined as

$$2k_j^T = \bar{\lambda}_T\cdot\bar{n}_j, \tag{5}$$

where $\bar{n}_j$ is the inward normal of each edge of the triangle with a magnitude equal to its length (see Fig. 5). In the air bearing problem, k_j^T only needs to be calculated once and stored for later use.

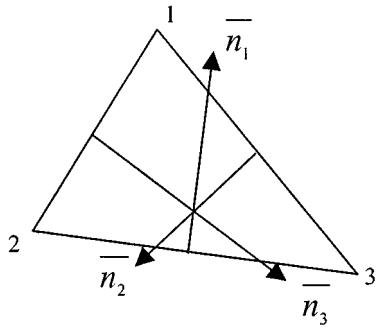

FIG. 5. The inward normals of a triangle.

The residual of each triangle is distributed to its nodes by the distribution coefficient β_i^T

$$\phi_i^T = \beta_i^T \phi^T. \tag{6}$$

The convection equation can be discretized as

$$\frac{A_\Omega}{\Delta T}\left[(PH)_i^{n+1} - (PH)_i^n\right] = -\sum_{T=1}^{M} \phi_i^T = -\sum_{T=1}^{M} \beta_i^T \phi^T = -\sum_{T=1}^{M} \beta_i^T \sum_{j=1}^{3} k_j^T (PH)_j^{n+1}, \tag{7}$$

where A_Ω is the area of the median dual and M is the number of triangles with i as one node. In the above formulation, the solution is updated by accumulating the residuals at node i, triangle by triangle. To put the schemes in a form that is convenient for the following multigrid iterations, we reformulated it such that the solution can be updated edge by edge

$$\begin{aligned}\frac{A_\Omega}{\Delta T}\left[(PH)_i^{n+1} - (PH)_i^n\right] &= -\sum_{T=1}^{M} \beta_i^T \sum_{j=1}^{3} k_j^T (PH)_j^{n+1} \\ &= -\sum_{j=1}^{M} \left[\left(\beta_i^{T_1} k_i^{T_1} + \beta_i^{T_2} k_i^{T_2}\right)(PH)_i^{n+1}\right. \\ &\quad \left. + \left(\beta_i^{T_1} k_j^{T_1} + \beta_i^{T_2} k_j^{T_2}\right)(PH)_j^{n+1}\right],\end{aligned} \tag{8}$$

where T_1 and T_2 are the two neigboring triangles sharing the edge ij.

For the PSI scheme [3, 4], the distribution coefficient can be written as

$$\beta_i^T = \frac{\max\left(0, k_i^T\right) \min(0, ((PH)_i - (PH)_{in})\phi^T)}{\sum_{j=1}^{3} \max\left(0, k_j^T\right) \min(0, ((PH)_j - (PH)_{in})\phi^T)}, \tag{9}$$

where $(PH)_{in}$ is the linearly interpolated PH value at the inflow point, which can be evaluated as

$$(PH)_{in} = \frac{\sum_{j=1}^{3} \min\left(0, k_j^T\right)(PH)_j}{\sum_{j=1}^{3} \min\left(0, k_j^T\right)}. \tag{10}$$

For the SUPG finite element scheme [5] in residual distribution form [6], the distribution coefficient can be written as

$$\beta_i^T = \frac{1}{3} + 0.5\frac{h}{|\lambda_T| A_T} k_i^T, \tag{11}$$

in which the length scale h can be approximated as

$$h = \max_{i=1}^{3}(|(n_i)_x|, |(n_i)_y|). \tag{12}$$

5. THE FINITE-ELEMENT DISCRETIZATION OF THE DIFFUSION TERMS

The diffusion terms are discretized using a Galerkin weighted integral [7]

$$\iint_{A_\Omega} \left[\nabla \cdot \left(QPH^3 \frac{\partial P}{\partial x}, QPH^3 \frac{\partial P}{\partial y}\right)\right] \frac{dA}{\sigma} = \sum_{j=1}^{M} W_{ij}\left[(P)_j^{n+1} - (P)_i^{n+1}\right]. \tag{13}$$

Here the weights W_{ij} are defined as

$$2\sigma W_{ij} = \overline{QPH^3}^L \cot an(\alpha_{Lj}) + \overline{QPH^3}^R \cot an(\alpha_{Rj}), \tag{14}$$

where $\overline{QPH^3}^L$ and $\overline{QPH^3}^R$ are the average values of QPH^3 in the triangle to the left or right of the edge ij. The terms α_{Lj} and α_{Rj} are the opposite angles to the edge ij as shown in Fig. 6.

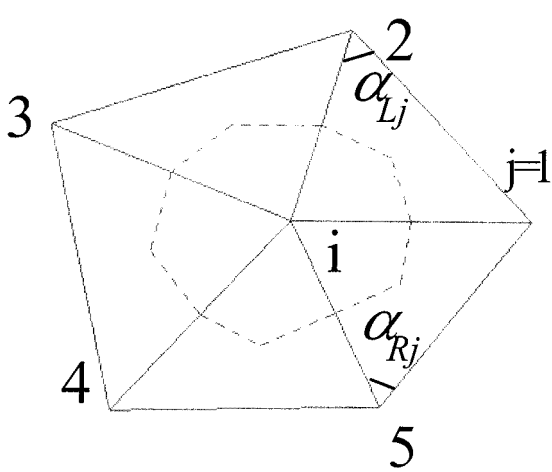

FIG. 6. The median dual control volume.

6. ITERATIVE SOLVER OF THE DISCRETIZED EQUATIONS

All of the above numerical schemes can be written in a unified form as

$$C_i P_i^{n+1} + \sum_{j=1}^{M} C_{ij} P_j^{n+1} = S_i\left(P_i^n, P_j^n\right), \tag{15}$$

where

$$C_i = \frac{A_\Omega}{\Delta T} H_i + \sum_{j=1}^{M} \left(\beta_i^{T_1} k_i^{T_1} + \beta_i^{T_2} k_i^{T_2}\right) H_i + \sum_{j=1}^{M} W_{ij}, \tag{16}$$

$$C_{ij} = \left(\beta_i^{T_1} k_j^{T_1} + \beta_i^{T_2} k_j^{T_2}\right) H_j - W_{ij}, \tag{17}$$

$$S_i\left(P_i^n, P_j^n\right) = \frac{A_\Omega}{\Delta T} (PH)_i^n. \tag{18}$$

Equation (15) is still nonlinear, because C_i and C_{ij} depend on P^{n+1}. One simple way to linearize the equation is to take P as the most recent known value of the last iteration. This is the so-called lagging technique. The resulting simultaneous equations are solved by a two sweep point Gauss–Seidel method. The first sweep starts from the beginning of the vertex list, and the second sweep starts from the end of the list. This takes into account the fact that the diffision terms in the Reynolds equation are elliptic in nature, and disturbance information is spread simultaneously in all directions.

The solution for one fixed slider attitude is found by marching in time. For problems with fixed attitude, the unsteady term is not needed as part of the solution, but it is kept here to serve as an underrelaxation term. When a relatively large time step is used, the unsteady term can be ignored, and the technique is more like a direct iteration than time marching. The implicit schemes are unconditionally stable, so an arbitrarily large CFL number such as 1.0E12 can be used.

7. GRID TRANSFER OPERATORS FOR THE MULTIGRID ALGORITHM

In the implementation of the multigrid algorithm, the variables, residues, and corrections are transferred frequently between different mesh levels. The transfer procedure has vital influence on the overall performance of the multigrid algorithm. Mavripilis and Jameson's [9] grid transfer operators are proven to be well suited for multigrid algorithms over non-nested unstructured triangular meshes. Here we simply adopt their operators.

When the restriction operator is applied to the variables, the operation can be taken as a linear interpolation of the variables from the fine mesh nodes to the coarser mesh nodes. If it operates on the residue, then the residue at the vertex of finer meshes can be distributed to the three vertices of the coaser triangle that encloses the vertex by its three area coordinates. This guarantees the conservation of the residual in the transfer process.

The interpolation operator is used to transfer corrections from the coarser meshes to the finer meshes. It can simply be taken as a linear interpolation.

8. FAS MULTIGRID ALGORITHM

The full approximation storage (FAS) algorithm in Brandt [8] is well suited for nonlinear equations. It solves the equations by iterating over several sets of meshes. In our actual implementation, three levels of meshes are used. Figure 7 shows the multigrid V cycles used in the simulation. The number in each circle represents the number of iterations done on that mesh level. At the beginning of each iteration, the coefficents of the equation are updated once and stored using the solution of the previous time step, and the resulting linear algebraic equations are solved by a fixed number of two sweep Gauss–Seidel iterations. In our code, about 10 to 20 Gauss–Seidel iterations are used to find an approximate solution. To get a good initial guess we first perform 40 iterations on the coarsest meshes, then we linearly interpolate the solution variables to the second-level meshes. Twenty iterations are carried out there before we interpolate the solution variables to the third-level meshes where the standard V circle begins. NV cycles are carried out over the initial three sets of meshes to reduce the error to a certain level before we adaptively refine the third-level meshes according to the pressure distribution. The following V cycles are performed over the new finest meshes and the other two meshes until convergence is achieved. The number of iterations on each mesh level shown in the circle of Fig. 7 corresponds to the optimized convergence speed for some sliders.

9. INVERSE PROBLEM

In air bearing simulation, the balanced steady state flying attitude of the slider corresponding to a fixed prescribed load is more important than the air bearing pressure distribution of the steady state solution of one fixed attitude, because it is the former that is prescribed in the design of hard disk drives. The steady state flying attitude is defined as the one at which the pre-enforced suspension force and pitch and roll torques are balanced by their counterparts generated by the air bearing that are functions of flying attitude. We can define a vector $R = (R_1, R_2, R_3)$ with

$$R_1 = F_{air} - F_s, \tag{19}$$

$$R_2 = (M_{air})_p + (M_s)_p + (M_{shear})_p, \tag{20}$$

$$R_3 = (M_{air})_r + (M_s)_r + (M_{shear})_r, \tag{21}$$

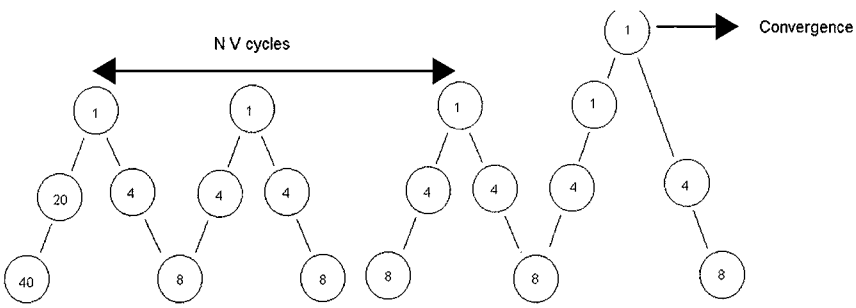

FIG. 7. The multigrid V cycles.

where F_{air} is the resultant air bearing force of a guessed flying attitude, F_s is the applied suspension force, M_{air}, M_{shear}, and M_s are moments caused by air bearing pressure, viscous shear force at the slider air bearing surface at that guessed attitude and the suspension, respectively. Subscripts p and r represent the projection in the pitch and roll directions (see Fig. 2). In Fukui and Kaneko's paper [13], the velocity profile at each modified inverse Knudsen number is not available, and as a result the shear moments cannot be evaluated. But for most sliders, the moments caused by viscous shears are very small compared to those caused by air bearing pressure. For example, as will be shown in the slider design in Fig. 4, which is free of suspension moments, at the inner radial position (15 mm), the viscous shear moments only account for 1.9% and 0.04% of the total in the pitch and roll directions, respectively. In addition, the difference between the velocity profile predicted by the first-order slip model and the Fukui and Kaneko model is also small. To simplify the problem, the velocity profile predicted by the first-order slip model [11] is used to evaluate the moments caused by viscous shear at the slider surface

$$(M_{shear})_p = P_a L h_m Z \int_0^b \int_0^1 \left(\frac{H}{2} \frac{\partial P}{\partial X} + \frac{\Lambda_x}{6(H + 2K_n)} \right) dX\, dY, \tag{22}$$

$$(M_{shear})_r = P_a L h_m Z \int_0^b \int_0^1 \left(\frac{H}{2} \frac{\partial P}{\partial Y} + \frac{\Lambda_y}{6(H + 2K_n)} \right) dX\, dY, \tag{23}$$

where Z is the thickness of the slider, and b is the dimesionless length of the slider. $K_n = \lambda / h_m$ is the Knudsen number with λ being the mean free path of air molecules, and R is a nonlinear function of the flying height, the pitch angle and the roll angle. The object is to find a particular flying attitude that makes R zero, which corresponds to the steady state flying attitude. The Quasi–Newton iteration method (Broyden's method) for nonlinear problems fully described in Dennis and Schnabel [10] is implemented to find the steady state flying attitude. Within each Quasi–Newton iteration, the air bearing force and moments are integrated from the pressure field calculated by the method presented

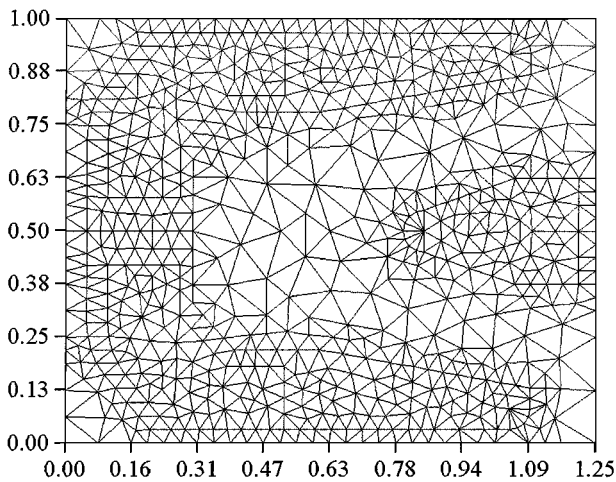

FIG. 8. The first-level conforming meshes with 717 nodes.

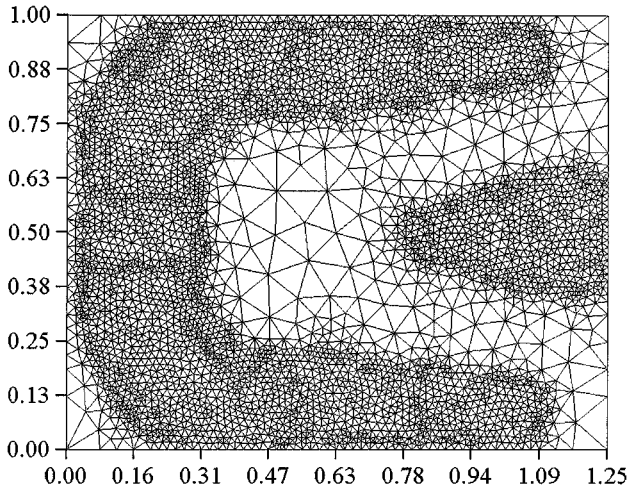

FIG. 9. The second-level meshes with 4245 nodes.

previously corresponding to the guessed attitude predicted by the Quasi–Newton step, the viscous shear moments are evaluated using (22) and (23). Our experience shows that generally only three to four Newton steps are needed to find the balanced steady state attitude, depending on the initially assumed values.

10. RESULTS AND DISCUSSION

Figures 3 and 4 depict a slider design intended to operate at a flying height of 5–10 nm. The length and width in the figures have been normalized by the dimensional width (1 mm), and the x- and y-coordinates in all the figures shown afterwards are dimensionless. Figures 8–10 show the three initial meshes used in the simulation. Figure 11 shows the adaptively refined

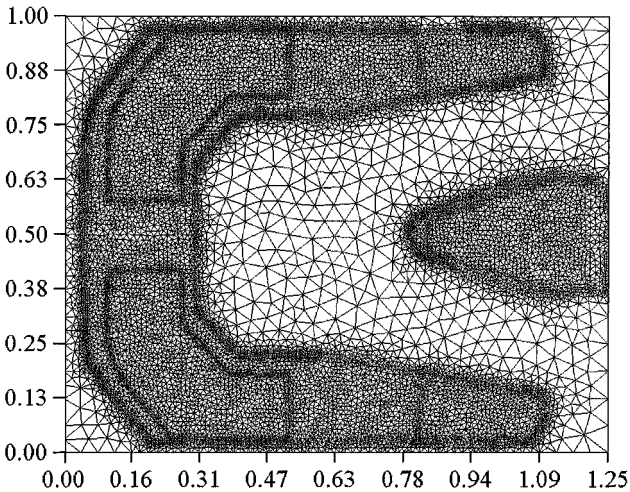

FIG. 10. The third-level meshes before mesh adaptation with 12612 nodes.

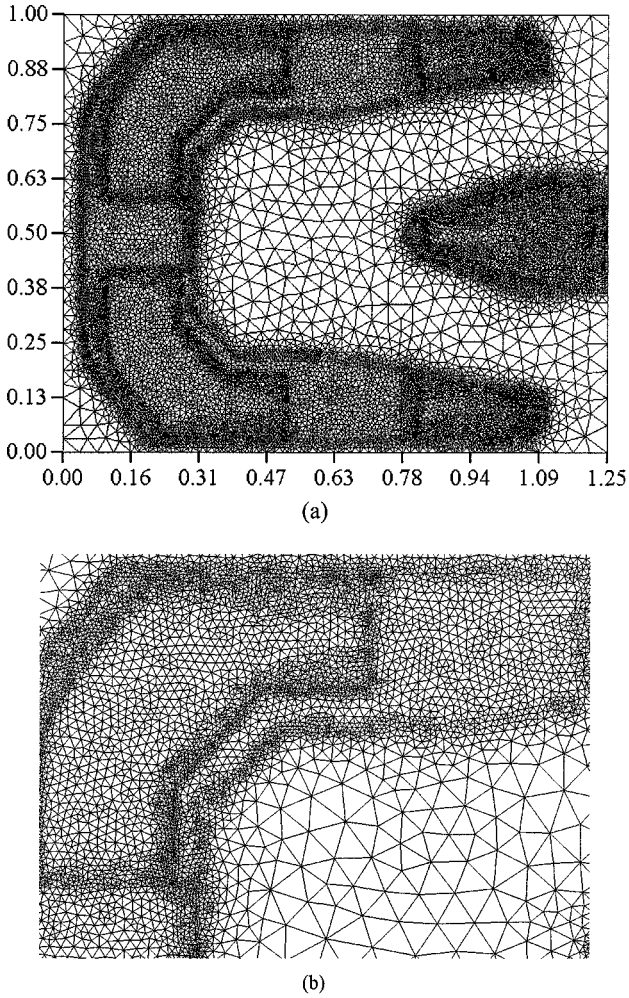

FIG. 11. The third-level meshes after mesh adaptation with 18112 nodes.

third-level meshes. From the above figures we see that all the regions with large geometric changes or pressure gradients have been efficiently captured by the mesh generation and adaptation techniques. Figure 12 shows the comparison of the convergence histories of the iterations on a single set of meshes and the multigrid iteration of solving the generalized Reynolds equation at a guessed attitude. The 'S' at the legend end represents the iteration on a single set of meshes, while the 'M' represents multigrid iteration. The convergence difference among the different schemes is very small, and it is almost undetectable for the single mesh iteration from the figure. The sudden error jump in the curve corresponds to mesh adaptation. From the figure it is seen that for the single mesh iteration, the error initially drops very fast. Only 10 iterations are needed to bring the error down from about $10^{-2.5}$ to 10^{-4}. But after the high-frequency error has been smoothed out, the curve flattens. It takes more than 140 iterations to further reduce the error by about two orders of magnitude. The multigrid curve shows that all error components can be efficiently removed. The log error drops almost linearly with the number of iterations (time steps). The figure also shows that the multigrid technique works well for both schemes on the triangular meshes. For this

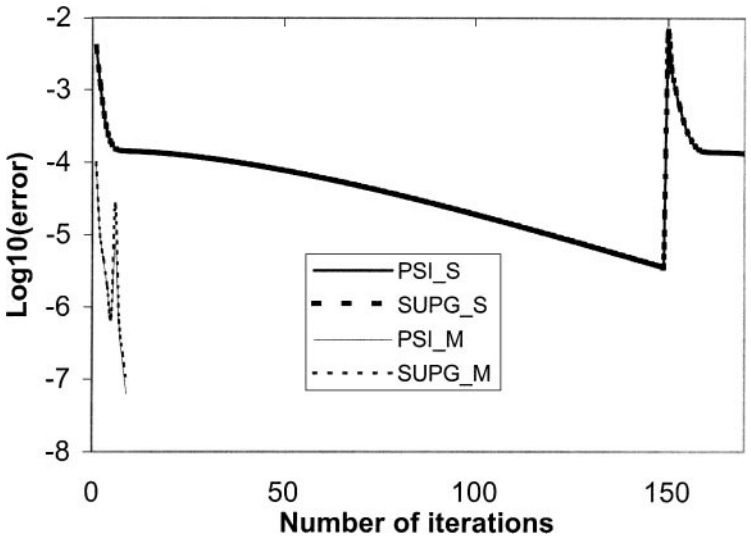

FIG. 12. The convergence comparison between the iteration on a single set of meshes and that of the multigrid iteration for different schemes.

particular slider, only seven multigrid cycles are needed to get the converged solution. More than one order of magnitude of simulation time is saved by use of the multigrid technique.

Figures 13 and 14 show the air bearing pressure contours at the steady state attitude obtained by the PSI and SUPG schemes, respectively. The disk is rotating at 7200 RPM, and the slider is located at a 15 mm radial position with a -1.22 μRad skew angle. The

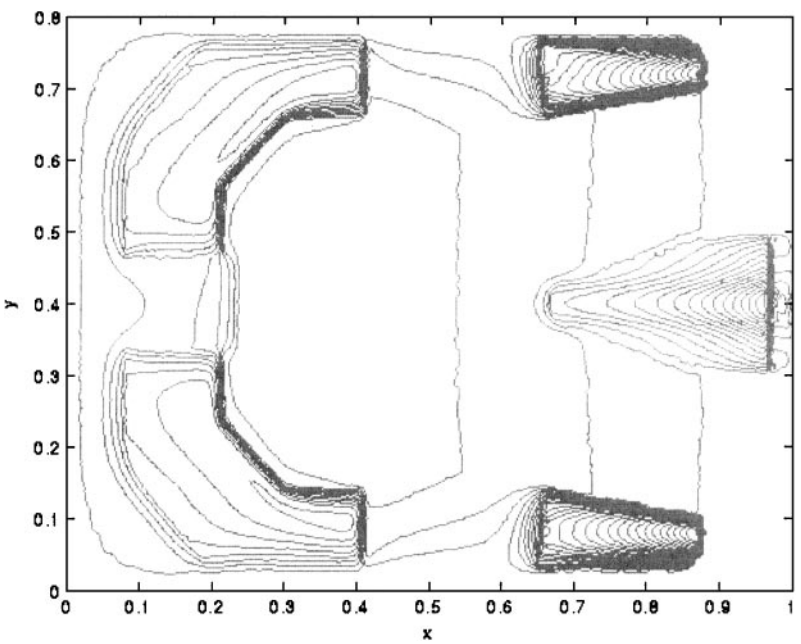

FIG. 13. The pressure contour calculated by the PSI scheme with 18110 nodes for the finest level meshes.

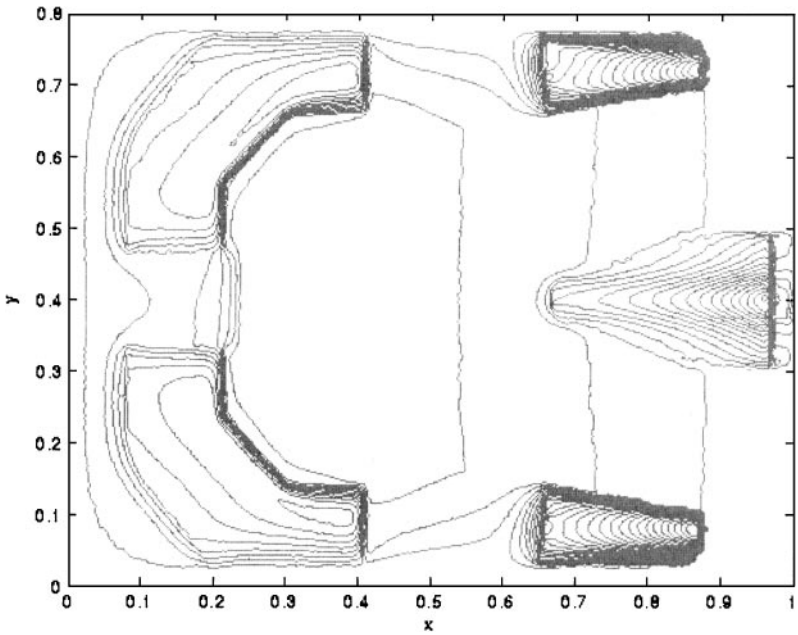

FIG. 14. The pressure contour calculated by the SUPG scheme with 18110 nodes for the finest level meshes.

prescribed suspension force is 14.7 mN at the center of the slider, the prescribed suspension torques are zero. The pressure contours differ only by very small details.

Figure 15 shows the flying height grid convergence history of the final steady state flying height. The results predicted by the two schemes agree with each other very well. Both schemes show a trend to converge to an 8-nm flying height. Figures 16 and 17 show the pitch angle and roll angle grid convergence histories, respectively. For the number of nodes corresponding to flying height convergence, all schemes reach grid convergence. Figure 18

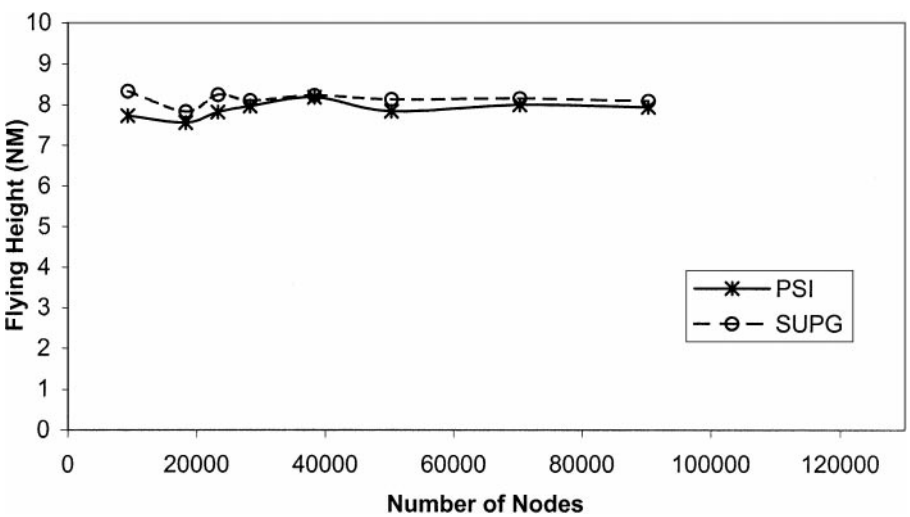

FIG. 15. The grid convergence of nominal flying height for different schemes.

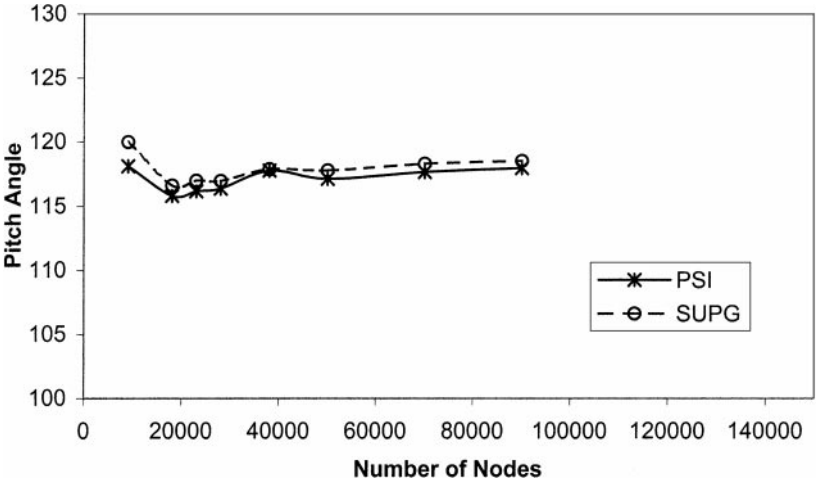

FIG. 16. The grid convergence of the pitch angle (μRad) for different schemes.

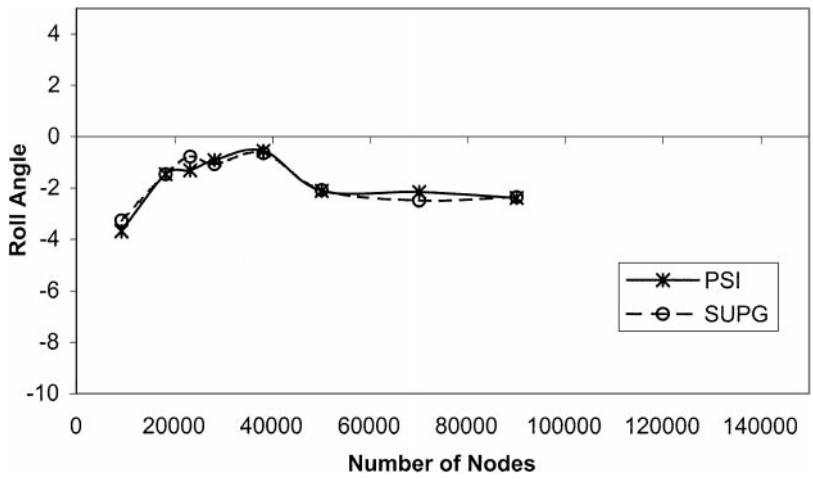

FIG. 17. The grid convergence of the roll angle (μRad) for different schemes.

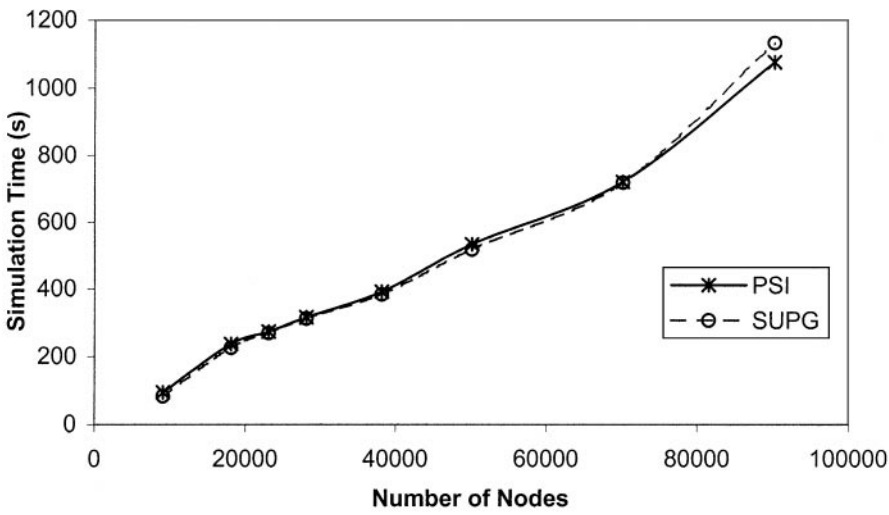

FIG. 18. The simulation time on a PII 350 PC as a function of number of nodes.

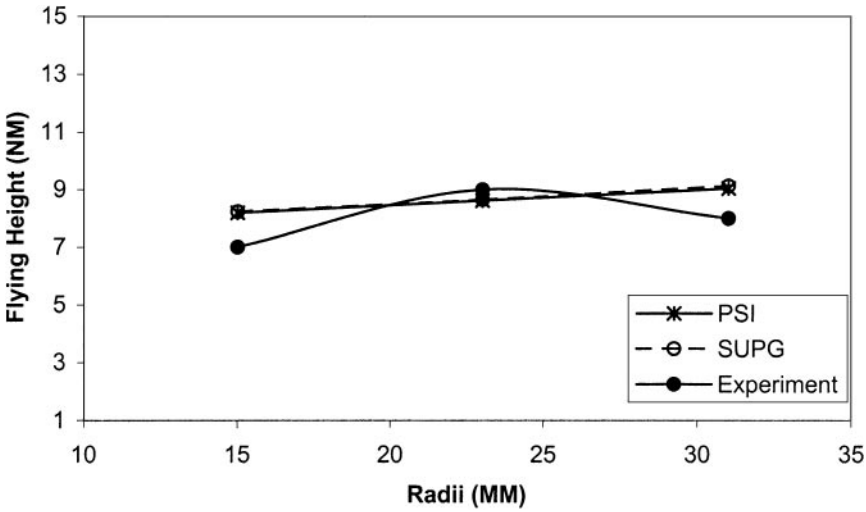

FIG. 19. The flying height at different radial position for the NSIC slider.

shows a plot of the simulation time for finding the steady state attitude as a function of the grid size.

Figure 19 compares the steady state flying heights of the slider at three radial positions obtained by the two numerical schemes with experimental measurements using a slider fabricated from this design. The results predicted by both numerical schemes are quite close to the experimental data, and the small differences between the numerical simulations and the experiments are within the error limit of experiments.

11. SUMMARY AND CONCLUSIONS

Two numerical schemes are used to discretize the convection part of the generalized Reynolds equation on unstructured triangular meshes. One is the PSI scheme, another one is the SUPG scheme. For the Reynolds equation the unknown is the pressure P, but to keep the convection equation in conserved form, we take PH as the variable in the discretization of the convection part. The known spacing H is taken out later to form the linearized simultaneous equations together with the contribution from the strongly nonlinear diffusion parts, which are disretized by a linear Galerkin finite element method. The Reynolds equation is characterized by extremely strong convection effects in hard disk drives, the bearing number is usually in the order of 10^3. The geometry of the air bearing slider changes dramatically in a very narrow wall profile region. The dimension of the slider is about 1 mm, while the horizontal scale of the wall profile region is about 10 μm. Within this narrow region, the pressure normally changes from several atmospheres at the bearing surface to ambient or subambient at the fully recessed region. As a result, an extremely large pressure gradient is built up. To accurately resolve the pressure profile is essential to obtaining the accurate flying attitude. This requires that the numerical scheme used to discretize the convection equation introduce as little numerical diffusion error as possible, otherwise very large amounts of meshes have to be used before the grid converged results can be obtained.

In a previous code developed by Lu [19] for the slider design used here, apparent increasing of flying height with the increasing of the mesh number is still observed even when a 385×385 grid system is used. Lu's code is based on the hybrid finite volume scheme for convection and diffusion equation of Patankar [20]. The current approach requires much fewer meshes to achieve grid convergence; this demonstrates that the PSI or SUPG descretization of the convection equation together with the Galerkin treatment of the diffusion parts are more accurate in solving the generalized Reynolds equation. The resulting numerical schemes are shown to be unconditionally stable. A non-nested FAS multigrid algorithm has been successfully employed to speed up the convergence rate of the schemes. The multigrid algorithm requires no relationship between different mesh levels, but the relationship has influence on the covergence speed. Nearly one order of simulation time is saved by implementing the multigrid algorithm. Even though the current code is based on unstructured meshes, which costs large amount of time to access data through a complicated data structure, its convergence speed can compete with Lu's code [19], which uses a structured rectangular mesh system and the same multigrid strategy of Brandt [8], even with a similar mesh number. This demonstrates that Brandt's FAS multigrid algorithm is very robust and that Mavriplis and Jameson's grid transfer operators are well suited for unstructured mesh systems. The steady state flying attitude is found by a Quasi–Newton iteration method (Broyden's method). Although the mesh number required by the slider air bearing problem both physically and numerically is very large compared with other two-dimensional problems, the current code requires only about two to three minutes on a PII350 PC (with a node number of about 18000) to find the acceptable final converged steady state flying attitude for most sliders used in the industry. The results predicted by the code agree well with experimental data.

ACKNOWLEDGMENTS

This work was supported by the Computer Mechanics Laboratory at University of California at Berkeley.

REFERENCES

1. L. Wu and D. B. Bogy, Unstructured triangular mesh generation techniques and a finite volume numerical scheme for slider air bearing simulation with complex shaped rails, *IEEE Trans. Magn.* **35**, 2421 (1999).
2. L. Wu and D. B. Bogy, Unstructured adaptive triangular mesh generation techniques and finite volume schemes for slider air bearing problems in hard disk drives, *ASME J. Tribology* **122**, 761 (2000).
3. R. Struijs, H. Deconinck, and P. L. Roe, Fluctuation splitting schemes for the 2D Euler equations, in *Proceedings of the VKI Lecture Series on Computational Fluid Dynamics, VKI LS 1991-01* (1991).
4. H. Paillere, H. Deconinck, and A. Bonfiglioli, A linearity-preserving wave-model for the solution of the Euler equations on unstructured meshes, in *Proceedings of the 2nd European CFD Conference, Stuttgart 1994.*
5. T. J. R. Hughes and A. N. Brooks, *Finite Element Methods for Convection Dominated Flows* (ASME, New York, 1979), Vol 34.
6. H. Deconinck, R. Struijs, G. Bourgois, and P. L. Roe, Compact advection schemes on unstructured grids, *Proceedings of the VKI Lecture Series on Computational Fluid Dynamics, VKI LS 1993-04* (1993).
7. T. J. Barth, *Numerical Aspects of Computing Viscous High Reynolds Number Flows on Unstructured Meshes*, Technical Paper 91-0721 (AIAA Press, Washington DC, 1991).
8. A. Brandt, Multi-level adaptive solutions to boundary value problems, *Math. Comp.* **31**, 333 (1977).
9. D. Mavriplis and A. Jameson, *Multigrid Solution of the Two-Dimensional Euler Equations on Unstructured Triangular Meshes*, Technical Paper 87-0353 (AIAA Press, Washington, DC, 1987).

10. J. E. Dennis and R. B. Schnabel, *Numerical Methods for Unconstrained Optimization and Nonlinear Equations*, Prentice-Hall, Englewood Cliffs, NJ (1983).
11. A. Burgdorfer, The Influence of the molecular mean free path on the performance of hydrodynamic gas lubricated bearings. *ASME J. Basic Eng.* **81**, 94 (1959).
12. Y. T. Hsia and G. A. Domoto, An experimental investigation of molecular rarefaction effects in gas lubricated bearings at ultra-low clearances, *ASME J. Lubr. Technol.* **105**, 120 (1983).
13. S. Fukui and R. Kaneko, A database for interpolation of Poiseuille flow rates for high knudsen number lubrication problems, *ASME J. Tribology* **110**, 335 (1988).
14. F. J. Alexander, A. L. Garcia, and B. J. Alder, Direct simulation Monte Carlo for thin-film bearings, *Phys. Fluids* **6**, 3854 (1994).
15. W. Huang, D. B. Bogy, and A. L. Garcia, Three-dimensional direct simulation Monte Carlo method for slider air bearings, *Phys. Fluids* **9**, 1764 (1997).
16. S. W. Sloan, A Fast Algorithm for constructing Delaunay triangulations in the plane, *Adv. Eng. Software* **9**, 34 (1987).
17. J. Ruppert, A Delaunay refinement algorithm for quality 2-dimensional mesh generation, *J. Algorithms* **18**, 548 (1995).
18. M. Rivara and P. Inostroza, Using longest-side bisection techniques for the automatic refinement of Delaunay triangulations, *Int. J. Numer. Meth.* Eng. **40**, 581 (1997).
19. S. Lu, *Numerical Simulation of Slider Air Bearings*, Doctoral dissertation, Department of Mechanical Engineering, University of California, Berkeley (1997).
20. S. V. Patankar, *Numerical Heat Transfer and Fluid Flow* (McGraw-Hill, New York, 1980).